applied sciences

MDPI

Article

Polyadic Cantor Fractal Ultrasonic Lenses: Design and Characterization

Sergio Castiñeira-Ibáñez [1], Daniel Tarrazó-Serrano [2], Jose Miguel Fuster [3], Pilar Candelas [2] and Constanza Rubio [2,*]

1 Departamento de Física Aplicada, Universitat Politècnica de València, Camí de Vera s/n, 46022 València, Spain; sercasib@upvnet.upv.es
2 Centro de Tecnologías Físicas, Universitat Politècnica de València, Camí de Vera s/n, 46022 València, Spain; dtarrazo@fis.upv.es (D.T.-S.); pcandelas@fis.upv.es (P.C.)
3 ETSI de Telecomunicación, Universitat Politècnica de València, Camí de Vera s/n, 46022 València, Spain; jfuster@dcom.upv.es
* Correspondence: crubiom@fis.upv.es

Received: 5 July 2018; Accepted: 15 August 2018; Published: 17 August 2018

Abstract: Traditional acoustic lenses modulate the ultrasonic beam due to their curved surfaces and the refractive material of which they are made. In this work, a different type of acoustic lens, based on Polyadic Cantor Fractals (PCF), is presented and thoroughly analyzed. These new Polyadic Cantor Fractal Lenses (PCFLs) are completely flat and easy to build, and they present interesting modulation capabilities over the acoustic profile. The dependence of the focusing profile on the PCFL design parameters is fully characterized, and it is shown that certain design parameters provide a dynamic control, which is critical in many medical applications such as thermal ablation of tumors.

Keywords: fractal lenses; diffraction; polyadic Cantor fractal; ultrasonics

1. Introduction

The diffraction phenomenon has been traditionally used to control beamforming and focalization of lenses in different physical fields such as optics, acoustics or microwaves. Conventional lenses' focusing capabilities are based on their curved shapes and their refractive materials. As an alternative to traditional lenses, different solutions have been investigated such as sonic crystals [1], planar structures built with concentric rings such as Fresnel lenses [2] or variations on the latter, pinhole zone plates [3]. It has been shown that these new lenses can improve focalization over traditional ones.

In the acoustic field, the modulation control of acoustic beams is an important topic, because it can result in a significant advance in different applications such as medical therapy or non-destructive material analysis, which includes a wide range of areas such as material flaw detection [4], pest detection in agroforestry [5] and food analysis [6].

The use of planar structures that are capable of guiding and focusing waves the same way as traditional lenses is very interesting. Among the possible geometries that can be analyzed, fractal structures have already been proposed [7,8]. Particularly, Generalized Polyadic Cantor Sets (GPCSs) are very attractive because they can be generated with simple algorithms, and this is the main reason why the majority of studies are based on these type of fractals [9,10]. Fractal lenses have been shown to become a possible improvement on focalization properties, reducing aberration simultaneously [11].

In this work, the design and characterization of planar acoustic lenses based on GPCSs is developed, and their application as ultrasonic lenses is analyzed. These new kinds of lenses are known as Polyadic Cantor Fractal Lenses (PCFLs). These structures are proposed because of their ease of fabrication and their multifocus profile.

2. Polyadic Cantor Fractal Lens Generation

Figure 1 shows a Polyadic Cantor Fractal Lens (PCFL) across the XY-coordinate plane with plane wave excitation. The acoustic field is modulated by the lens and originates a focus on a perpendicular axis to the lens. The distance between the position of the focus and the lens plane is known as the focal distance (FL). In some applications, it may be necessary to have multiple foci.

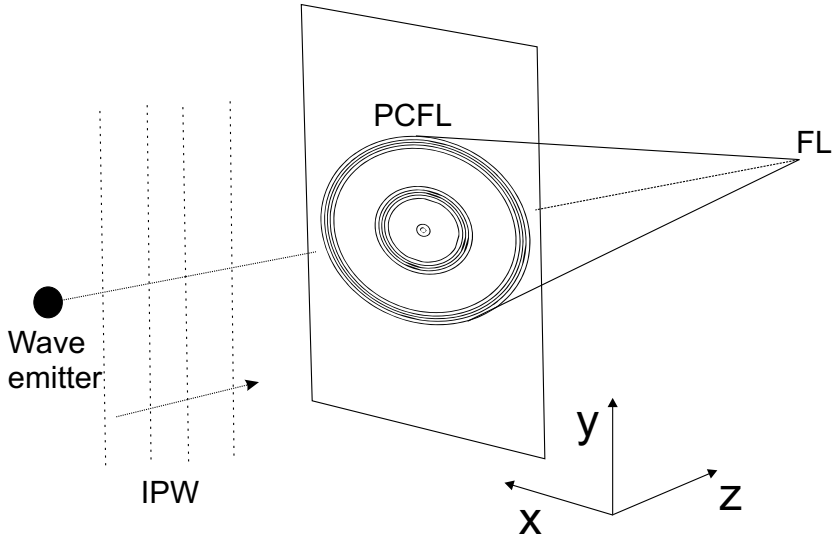

Figure 1. Polyadic Cantor Fractal Lens (PCFL) built with concentric rings. The lens focus is located in an axis orthogonal to the lens plane at distance FL.

The PCFL is built using the GPCS algorithm. First, the initial element (stage $s = 0$), known as the initiator, is substituted by a set of N segments of identical lengths $W_0 = Lr$. The rparameter is known as the scaling factor and should take values from 0–1/2 in order to produce a GPCS; see Figure 2a. These segments are separated by gaps. If N is even, there is a central gap of width g_c and $N - 2$ lateral gaps of width ε; see Figure 2b. If N is odd, the central gap is split into two halves of width $g_c/2$ at the sides of the central segment, and there are $N - 3$ lateral gaps of width ε; see Figure 2c. As can be seen in Figure 2, the number of total gaps is always given by $n_{gaps} = N - 1$.

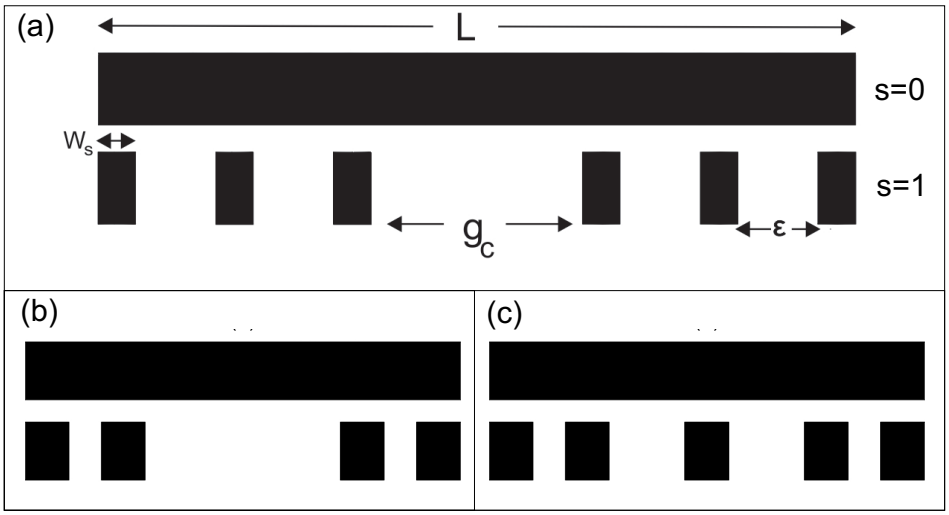

Figure 2. (**a**) GPCS main parameters, (**b**) even GPCS and (**c**) odd GPCS.

This way, the stage $s = 1$ of the GPCS, known as the generator, is constructed. Both the initiator ($s = 0$) and generator ($s = 1$) have exactly the same length. This procedure is repeated as many times as required in the following stages. The number, distribution and widths of the segments of the generator affect the homogeneity and texture of the fractal. To characterize these features, parameters such as the fractal dimension (D), the number of elements (N), the fractal stage s, the central gap width g_c and the lateral gap width ε are considered; see Figure 2a.

The fractal dimension is defined as,

$$D = -\frac{\ln(n_{gaps} + 1)}{\ln r} \tag{1}$$

with n_{gaps} the total number of gaps of the generator and r the scaling factor. If N is fixed, n_{gaps}, as well, and r must be modified to obtain different values for the fractal dimensions. Therefore, the fractal dimension relates directly to the transparency of the fractal.

An alternative way to refer to the fractal gap distribution is through a parameter known as the central gap fraction f_{gc}. This parameter ranges from 0–1 and gives an indication of the weight of the central gap over the total gap space in the generator. The width of the central gap can be related to the central gap fraction using,

$$g_c = L(1 - rN)f_{gc} \tag{2}$$

As mentioned above, the even-order GPCS has a unique central gap of width g_c, while the odd-order GPCS splits the central gap into two gaps of widths $g_c/2$ at both sides of the central segment. The lateral gap widths of the generator can be calculated with the following expressions,

$$\varepsilon = \begin{cases} \frac{L(1-Nr)-g_c}{N-2} & N \geq 4 \text{ if } N \text{ is even} \\ \\ \frac{L(1-Nr)-g_c}{N-3} & N \geq 5 \text{ if } N \text{ is odd} \end{cases} \tag{3}$$

As stated previously, this is a recursive procedure. In each stage, the different segments are substituted by generator copies of the same length. Thus, as the stage evolves, the number of segments increases, while the segment length decreases. At stage s, the segment lengths can be calculated with,

$$W_s = Lr^s \tag{4}$$

Although this iterative procedure can be repeated indefinitely, once the second stage ($s = 2$) is achieved, the iterative procedure is truncated due to mechanical limitations with the construction of the device. Therefore, the final structure is not a real fractal, but a prefractal.

The PFCL is then generated from the prefractal structure. In order to do that, the prefractal structure revolves 180 degrees around a perpendicular axis aligned through the center of the GPCS (OZ axis); see Figure 3a. In this way, a set of concentric rings is obtained at the OXY plane, as can be observed from Figure 3b. The PFCL generated in the OXY plane is shown in three dimensions in Figure 1.

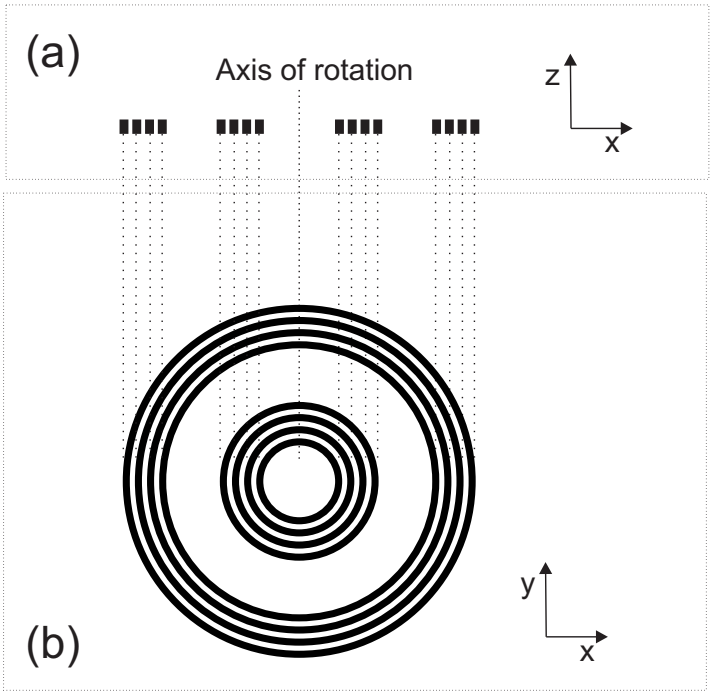

Figure 3. Lens generation from the Generalized Polyadic Cantor Set (GPCS), (**a**) prefractal GPCS at stage $s = 2$ and (**b**) planar PCFL obtained from revolution generation of the prefractal around its orthogonal axis.

3. Numerical Model

Nowadays, there is a large number of mathematical techniques that can be used for solving acoustic problems, taking into account the interaction of ultrasonic waves with structures immersed in water. In this work, the Finite Element Method (FEM), and in particular the commercial software COMSOL Multiphysics, has been used. This software is capable of solving complex geometries with multiple acoustic phenomena. To solve the acoustic problem, it is necessary to define the geometry to be analyzed, to implement the boundary conditions correctly and to discretize the resolution domain. For this purpose, it is necessary to solve the Helmholtz equation given by,

$$\nabla \left(\frac{-1}{\rho} \nabla p \right) = \frac{\omega^2}{\rho c^2} p \tag{5}$$

where ρ (ρ = 1000 kg/m^3) is the medium density, c (c = 1500 m/s) is the ultrasound velocity, ω is the angular frequency and p is the acoustic pressure.

Figure 4 shows the scheme of the numerical model. It is an ideal 2D axisymmetric model, which allows 2D analysis equivalent to a more complex 3D analysis, significantly reducing the calculation loads. Computation times are reduced, because the axisymmetric model takes advantage of the revolution symmetry of the problem, which is a direct consequence of the way the PCFL has been generated as described previously. Therefore, the software solves the acoustic problem by revolving 360 degrees around a perpendicular axis aligned through the center of the GPCS (OZ axis) the 2D model and obtaining a 3D equivalent, as shown in Figure 1.

The assumptions made in the simulations are the following: the wavelength of the incident plane wave is large compared to the thickness of the lens; the lens is considered to be acoustically rigid; therefore, the Neumann boundary condition, zero sound velocity, is applied, and finally, the plane wave radiation condition is also applied to the boundaries of the domain to simulate free space and emulate the Sommerfeld condition as shown in Figure 4. Due to the characteristics of the system that is being modeled, where small time-dependent pressure variation values are assumed, the so-called

background pressure field is considered. To quantify the acoustic field, the sound pressure level is calculated at each point in the domain, and then, the acoustic gain is calculated using the expression,

$$G_{focus} = 20 \cdot \log_{10} \left| \frac{p}{p_{incident}} \right| \tag{6}$$

where p is the sound pressure at an arbitrary point and $p_{incident}$ is incident sound pressure at the lens.

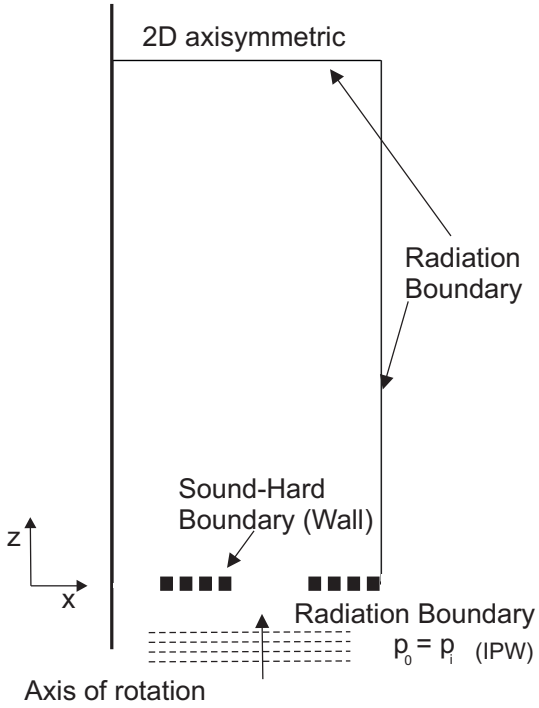

Figure 4. Schematic diagram of the numerical domain simulated configuration.

4. Results and Discussion

Once the PCFL design parameters have been presented, the influence of these parameters on the modulation of the sound beam is analyzed. For this purpose, the numeric method used in the previous section was employed. The design was oriented towards the fabrication of planar acoustic lenses with focal profile control mechanisms and beamforming capabilities. A lens of radius $R = L/2 = 12.5$ cm and negligible thickness compared with the wavelength was designed with the following design parameters: $D = 0.6$, $N = 5$, $f_{gc} = 0.4$. The operating frequency was set at $f = 100$ kHz. As mentioned above, for practical reasons and the ease of construction, the prefractal stage was set at $s = 2$.

The results that are going to be shown correspond to sound pressure gain maps in the OXZ plane, that is the plane orthogonal to the lens that contains its center. In this plane, the location, width and intensity of the different PCFL foci can be observed. The total width of the working space was equal to 20 cm along the OX axis, whereas 80 cm have been analyzed along the OZ axis from the position of the lens forward. In the pressure maps, the lens is located just at the bottom position ($z = 0$) of the OXZ plane.

Three different analyses have been carried out. First, the dependence of the focal distance on the operating frequency has been analyzed. Secondly, the influence of the fractal dimension on the focus location has been considered, and finally, the effect of the number of elements of the generator (N) on the focusing profile has also been studied.

4.1. Focusing Profile Variation with Frequency

Fixing the design parameters at values $R = 12.5$ cm, $D = 0.6$, $N = 5$ and $f_{gc} = 0.4$, the influence of the operating frequency variation on the PCFL focus location is analyzed. Figure 5 shows the layout of the PCFL to be analyzed. The lens is located at the OXY plane. The sound pressure gain map is obtained at the OXZ central plane in dB units.

The operating frequency is modified from 100 kHz–400 kHz. Figure 5 shows the simulated maps for four different frequencies. As can be observed from the figure, the location of the focus that is closer to the lens modifies its position when the operating frequency increases. This variation is linear and can be modeled with the following expression,

$$d_{focus}(f) = d_{focus}(100\text{ kHz}) \cdot \frac{f}{100\text{ kHz}} \tag{7}$$

with $d_{focus}(100\text{ kHz})$ the focal distance at an operating frequency of 100 kHz and f the operating frequency in kHz.

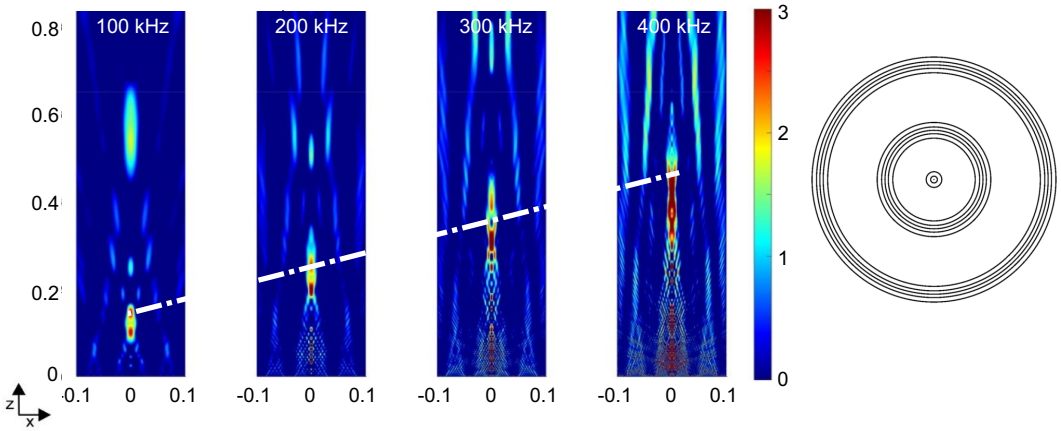

Figure 5. Focusing profile variation with frequency.

The graphical representation of Equation (7) is shown with a white line on Figure 5. It can be observed that it is a linear dependence. Once the PCFL is designed, a precise focus shifting along the Z-axis is achieved and controlled by slightly varying the operating frequency. Thus, a dynamic and effective mechanism to modify the PCFL focal length is provided.

4.2. Focusing Profile Variation with Fractal Dimension

Fixing the design parameters at values $R = 12.5$ cm, $f = 100$ kHz, $N = 5$ and $f_{gc} = 0.4$, the influence of the fractal dimension variation on the PCFL focusing profile is analyzed. Thus, fractal dimension has been modified between 0.5 and 0.8, with the results are shown in Figure 6. As can be observed, the foci location does not change. However, a significant increase of the sound intensity can be observed when the fractal dimension becomes higher.

From the figure, it can also be observed that the lens becomes less transparent when the fractal dimension increases. It can be concluded that the fractal dimension affects the gain of the main focus on the pressure map.

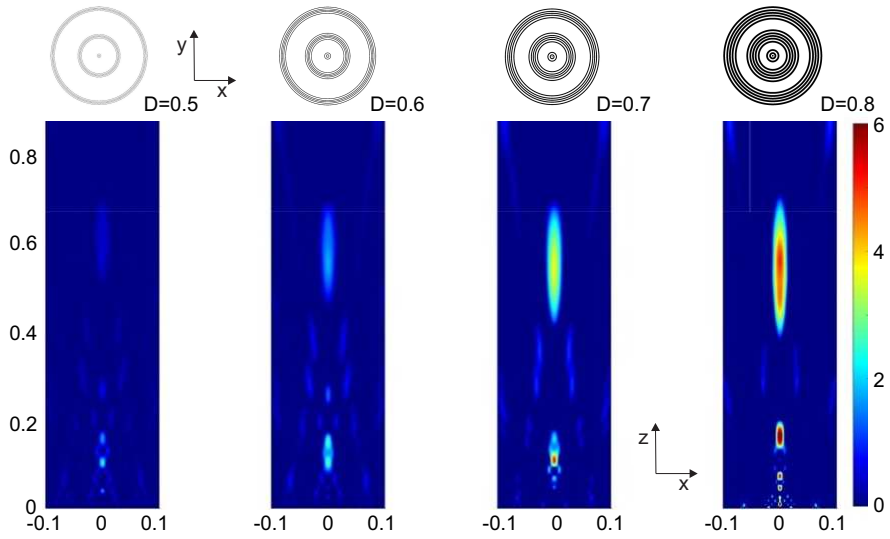

Figure 6. Focusing profile variation with fractal dimension.

4.3. Focusing Profile Variation with the Number of Elements

Fixing the design parameters at values $R = 12.5$ cm, $f = 100$ kHz, $D = 0.6$ and $f_{gc} = 0.4$, the influence of the number of elements of the generator on the PCFL beamforming capabilities is analyzed. This parameter has been modified between $N = 4$ and $N = 7$.

Table 1 shows the dependence of parameters r and g_c with N. Increasing N results in a decrease in r if the fractal dimension is kept constant, as a result of the elements becoming smaller. However, this inverse relationship is not linear, as can be observed in Equation (1) Therefore, the opacity percentage of the PCFL diminishes when N is increased, and the central gap becomes higher. Thus, increasing the number of elements N makes the lens slightly more transparent without requiring the variation of the fractal dimension; see Figure 7.

As can be observed from Figure 7, varying the number of elements (N) at Stage 1 ($s = 1$) allows one to enhance the gain of further or closer foci.

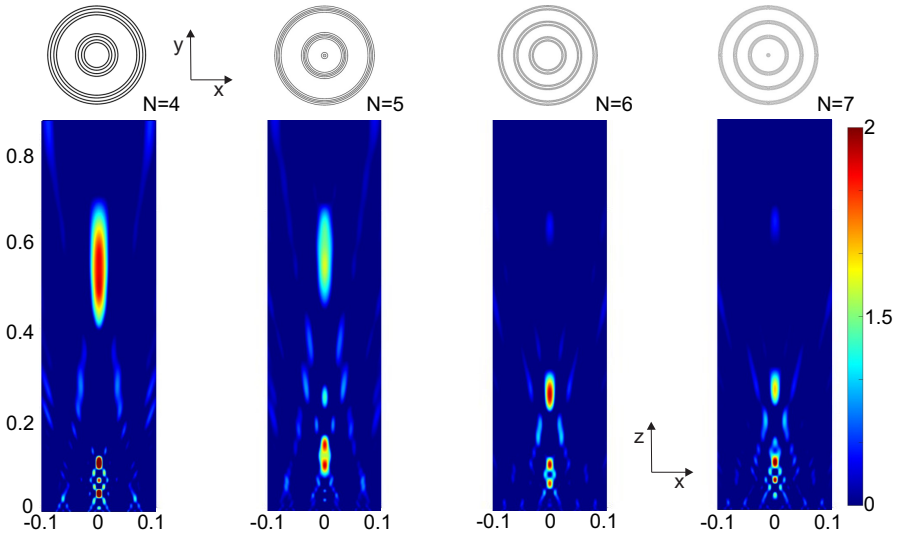

Figure 7. Focusing profile variation with the number of elements.

Table 1. Comparison of the different polyadic Cantor fractal lenses' parameter values.

N	f_{gc}	r	$g_c/2R$	D
4	0.4	0.099	0.241	0.6
5	0.4	0.068	0.263	0.6
6	0.4	0.050	0.278	0.6
7	0.4	0.039	0.290	0.6

5. Conclusions

In this work, a simple procedure for building planar lenses generated from fractal algorithms has been presented. These PCFLs allow us to modify and modulate their ultrasonic profiles. It has been shown that the fractal dimension parameter affects the gain of the principal focus on the pressure map and that modifying the number of elements of the generator results in an increase of the gain of secondary foci, giving full control of the PCFL focus profile. Moreover, a precise focus shifting is achieved along the Z-axis by slightly modifying the operating frequency, which gives the user a dynamic control parameter without modifying the lens. This dynamic control on the ultrasonic beam profile may be critical in certain medical applications such as thermal ablation of tumors.

Author Contributions: C.R. coordinated the theoretical developments and participated in the establishment of the theoretical principles used in this work and in the drafting of the manuscript. S.C.-I. and D.T.-S. developed the theory used, designed some of the computing tasks and participated in the drafting of the manuscript. J.M.F. and P.C. carried out the computing tasks and participated in the analysis of the state-of-the-art materials and in the drafting of the manuscript.

Funding: Spanish MINECO/FEDER (TEC2015-70939-R).

Acknowledgments: This work was supported by the Ministry of Economy, Industry and Competitiveness and the European Regional Development Fund TEC2015-70939-R (MINECO/FEDER).

Conflicts of Interest: The authors declare no conflict of interest.

References

1. Cervera, F.; Sanchis, L.; Sánchez-Pérez, J.V.; Martínez-Sala, R.; Rubio, C.; Meseguer, F.; López, C.; Caballero, D.; Sánchez-Dehesa, J. Refractive Acoustic Devices for Airborne Sound. *Phys. Rev. Lett.* **2001**, *88*, 023902. [CrossRef] [PubMed]
2. Calvo, D.C.; Thangawng, A.L.; Nicholas, M.; Layman, C.N. Thin Fresnel zone plate lenses for focusing underwater sound. *Appl. Phys. Lett.* **2015**, *107*, 014103. [CrossRef]
3. Rubio, C.; Fuster, J.M.; Castiñeira-Ibáñez, S.; Uris, A.; Belmar, F.; Candelas, P. Pinhole zone plate lens for ultrasound focusing. *Sensors* **2017**, *17*, 1690. [CrossRef] [PubMed]
4. Toh, S.L.; Shang, H.M.; Chau, F.S.; Tay, C.J. Flaw detection in composites using time-average shearography. *Opt. Laser Technol.* **1991**, *23*, 25–30. [CrossRef]
5. Gutiérrez, A.; Ruiz, V.; Moltó, E.; Tapia, G.; del Mar Téllez, M. Development of a bioacoustic sensor for the early detection of Red Palm Weevil (Rhynchophorus ferrugineus Olivier). *Crop Prot.* **2010**, *29*, 671–676. [CrossRef]
6. García-Pérez, J.; De Prados, M.; Benedito, J. Characterization of Pork Meat Products using Ultrasound. In *Ultrasound in Food Processing: Recent Advances*; John Wiley & Sons Ltd.: Hoboken, NJ, USA, 2017; pp. 86–114.
7. Castiñeira-Ibáñez, S.; Tarrazó-Serrano, D.; Rubio, C.; Candelas, P.; Uris, A. An Ultrasonic Lens Design Based on Prefractal Structures. *Symmetry* **2016**, *8*, 28. [CrossRef]
8. Castiñeira-Ibañez, S.; Tarrazó-Serrano, D.; Fuster, J.M.; Candelas, P.; Rubio, C. *Polyadic Cantor Fractals: Characterization, Generation, and Application as Ultrasonic Lenses*; InTech: Rijeka, Croatia, 2017; pp. 88–107.
9. Jaggard, A.D.; Jaggard, D.L. Cantor ring diffractals. *Opt. Commun.* **1998**, *158*, 141–148. [CrossRef]

10. Furlan, W.D.; Saavedra, G.; Monsoriu, J.A. White-light imaging with fractal zone plates. *Opt. Lett.* **2007**, *32*, 2109. [CrossRef] [PubMed]
11. Saavedra, G.; Furlan, W.D.; Monsoriu, J.A. Fractal zone plates. *Opt. Lett.* **2003**, *28*, 971. [CrossRef] [PubMed]